

Punctured-Chern topological invariants for semi-metallic bandstructures

Ankur Das,^{1,*} Eyal Cornfeld,¹ and Sumiran Pujari^{2,†}

¹*Department of Condensed Matter Physics, Weizmann Institute of Science, Rehovot 7610001, Israel*

²*Department of Physics, Indian Institute of Technology Bombay, Mumbai, MH 400076, India*

Topological insulator-based methods underpin the topological classification of gapped bands, including those surrounding semi-metallic nodal defects. However, multiple bands with gap-closing points can also possess non-trivial topology. We construct a general wavefunction-based “punctured-Chern” invariant to capture such topology. To show its general applicability, we analyze two systems with disparate gapless topology: 1) a recent two-dimensional fragile topological model to capture the various band-topological transitions and 2) a three-dimensional model with a triple-point nodal defect to characterize its semi-metallic topology with *half-integers* that govern physical observables such as anomalous transport. This invariant also gives the classification for Nexus triple-points ($\mathbb{Z} \times \mathbb{Z}$) with certain symmetry restrictions, which is re-confirmed by abstract algebra.

Electronic band topology has emerged as an important area of investigation following the realization that topological insulators are distinct than conventional band insulators [1–8]. Non-trivial topology of band structures arising from the underlying wavefunction geometry drives this phenomenology. This has made the topological classification of bands into an active field. This is done by formulating topological invariants that distinguish different band topologies, e.g. the familiar wavefunction-based Chern invariant [9]. They are generally described by different discrete groups [10–16].

Heretofore, such topological classification has primarily focused on insulating bands [1, 11–13], e.g. the \mathbb{Z}_2 topological insulator [17, 18]. Insulator-based classification is also used to characterize band degeneracies or nodes in one higher dimension by classifying gapped bands that surround such a node, e.g. Weyl points in $3d$ using $2d$ Chern classification [19], $2d$ Dirac points using $1d$ chiral insulator classification, etc. However, multiple bands may support non-trivial topology even in presence of gap-closing. A recent example is fragile topology that has arisen in the context of magic-angle twisted bilayer graphene [20–23]. It is understood as an obstruction to a localized Wannier representation that gets removed by addition of disconnected topologically trivial bands [24–27]. Such band topology arises also in presence of gap-closing points [21, 28]. The question then arises: how to characterize “gapless” topology, in particular by wavefunction-based invariants?

Recently, there has also emerged a new class of $3d$ semi-metals that host three-fold band degeneracies called Nexus triple-points [29, 30] where insulator-based methods again fail. These three-fold nodal defects have been predicted in several candidates [30–38] and seen in experiments on MoP [39], WC [40], and GeTe [41]. The failure results from the doubly-degenerate lines or nodal-lines that generically emanate from the triply-degenerate point (Fig. 3) and intersect with any enclosing surface necessarily, precluding surrounding gapped surfaces. The original papers (e.g. Refs. [29, 30]) had focused on insulator-based \mathbb{Z}_2 invariants on gapped $1d$ loops surrounding the

nodal-lines that gave the first inkling of the topology of Nexus defects. Another approach used quaternionic charges associated with nodal-chains for PT -symmetric models along with mirror symmetry [38] based on earlier works [42–44] that has been recently consolidated further [45, 46]. Both these approaches relied on the insulator-based paradigm on gapped $1d$ loops. Yet another attempt [47] that focused instead on the surrounding $2d$ gapless surface consisted of a homological characterization on a suitably extended manifold to account for analyticity everywhere. Formulating a wavefunction-based invariant directly on the (extended) manifold in one lower dimension surrounding the Nexus triple-point – similar in spirit to the Chern invariant – and its discrete group classification is desirable but yet to be formulated within the general scope of semi-metallic band topology.

Motivated by the considerations above, we construct below a wavefunction-based topological invariant employing Berry technology that is well-suited for semi-metallic bandstructures. We will demonstrate its utility through a $2d$ fragile topological model and a $3d$ Nexus triple-point model. This also will fill the classification gap for Nexus points for a specific set of symmetries. However, the invariant is more general and can be applied in other gap-closing contexts, including non-electronic ones. By the Chern theorem [48], the Chern number of a closed manifold has to be an integer. One way to compute the Chern number (Ch) of a $2d$ gapped band $|n\rangle$ is by using Berry connection \mathcal{A} and curvature Ω ,

$$\text{Ch}(n) = \frac{1}{2\pi} \int_{\mathbf{k} \in \mathcal{M}} \Omega_n d^2k, \quad (1)$$

with $\Omega_n = \frac{\partial}{\partial k_1} \mathcal{A}_2(n) - \frac{\partial}{\partial k_2} \mathcal{A}_1(n)$ and $\mathcal{A}_i(n) = i \langle n | \frac{\partial}{\partial k_i} | n \rangle$. If the manifold \mathcal{M} is not closed but has a boundary, then the Stokes theorem relates the curvature integral to the connection integral along the manifold boundary,

$$\gamma_n = \int_{\mathbf{k} \in \mathcal{M}} \Omega_n d^2k = \int_{\mathbf{k} \in \partial \mathcal{M}} \mathcal{A}(n) \cdot d\mathbf{k}. \quad (2)$$

This quantity, in general, does not have to be quantized. We study the case where our surface of interest is a punc-

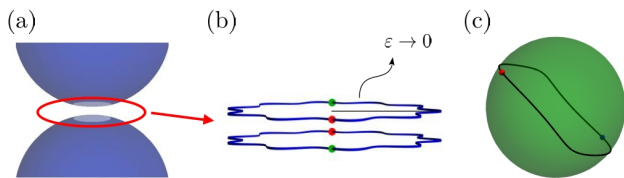


FIG. 1. (a) Representation of the extended manifold near a puncture due to the gap-closing between two bands [47]. (b) A zoom near the puncture on a piece of the manifold whose radius tends to zero. (c) Representation of the image on the $2d$ subspace (Bloch sphere) of this infinitesimal manifold. It illustrates the antipodal nature of the image independent of the shape of the infinitesimal piece in panel (b).

tured manifold. In particular, take a surface in the $3d$ \mathcal{BZ} which crosses one or more nodal-line band-crossings or a $2d$ \mathcal{BZ} with one or more gap closing points. The relevant bands cannot be uniquely defined where the gap closes. These surfaces should thus be considered as punctured, with a puncture imagined as an infinitesimal boundary circling the associated gap-closing point (Fig. 1). Let us consider first the contribution to Eq. 2 due to a single puncture involving two bands, say $|n\rangle$ and $|n+1\rangle$. If this puncture has a linear band-crossing, then the wavefunction $\Psi_n(\mathbf{k}(-s))$ is analytically connected with $\Psi_{n+1}(\mathbf{k}(s))$ for any curve $\{\mathbf{k}(s)\} \subset \mathcal{M}$ traversing around the puncture at $s = 0$ [47]. Since $\Psi_n(\mathbf{k}(s))$ is orthogonal to $\Psi_{n+1}(\mathbf{k}(s))$, it follows that $\Psi_n(\mathbf{k}(s = 0^-))$ is orthogonal to $\Psi_n(\mathbf{k}(s = 0^+))$, i.e. the wavefunction $\Psi_n(\mathbf{k})$ is orthogonal at antipodal points along the infinitesimal puncture circling the gap-closing point (Fig. 1).

The $2d$ subspace spanned by the two bands has the geometry of a Bloch sphere [49]. Perpendicular states are represented as antipodal points on the Bloch sphere. Thus the image on the Bloch sphere of the puncture is an antipodal trajectory (c.f. Fig. 1(c)). Since any antipodal trajectory necessarily divides the Bloch sphere into two equal halves, and the Bloch sphere includes an integer Berry flux; therefore, the antipodal trajectory divides the net Berry flux into two equal halves. This implies that the Berry flux associated with the antipodal trajectory is half-integer (in units of flux quantum). That is, *there is a half-integer contribution to the Chern number on the punctured manifold due to a puncture with a linear band-crossing*. As a corollary, a manifold that is punctured an odd number of times linearly will have a net half-integer Chern number. A natural case with such structures are Nexus triple-points to be seen later.

We first apply this ‘‘punctured-Chern’’ invariant to a $2d$ fragile topological model [28]. We focus here on capturing the gapless topology in the parameter space, a big swath of which has gap-closing points for all the bands. The model has four orbitals per unit cell (accounted by

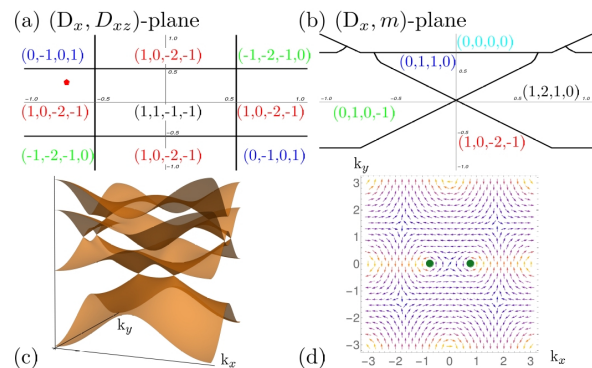


FIG. 2. (a) and (b) show the gapless band-topological phase diagrams in $\{D_x, D_{xz}\}$ and $\{D_x, m\}$ planes respectively for Eq. 3. The other parameters are held fixed ($t_1 = 1, t_2 = 0.5$; $m = -0.5$ for (a); $D_{xz} = 0.5$ for (b)). The transition between the regions (solid lines) with different punctured-Chern numbers are accompanied by additional gap-closing. (c) shows the dispersion for a specific point in the phase diagram marked by a red pentagon in (a). (d) shows the Berry connection map for the bottom band at this point with a non-zero punctured-Chern number (the first entry in the corresponding region).

σ and τ Pauli matrices), and the Bloch Hamiltonian is

$$H = d_z(\mathbf{k})\sigma_z + d_x(\mathbf{k})\tau_z\sigma_x + d_y(\mathbf{k})\sigma_y + D_x\tau_x + D_{xz}\tau_x\sigma_z \quad (3)$$

with $d_z(\mathbf{k}) = m + t_1(\sin^2(k_x/2) + \sin^2(k_y/2))$, $d_x(\mathbf{k}) = t_2 \sin(k_x)$, $d_y(\mathbf{k}) = t_2 \sin(k_y)$. The bandstructure at a particular point in the parameter space is shown in Fig. 2(c) with punctured-Chern invariant $(1, 0, -2, -1)$. Moving around in the parameter space keeps this invariant unchanged unless one crosses a boundary where additional gap-closing occurs (Fig. 2(a),(b)).

To visualize the gapless topology, we plot the Berry connection \mathcal{A} for a specific gapless band in Fig 2(d). This shows the *extra* sources and sinks of curvature that lead to the non-trivial topology. In contrast, a trivial punctured-Chern topology would be the nearest-neighbor hopping model for graphene. It has no extra sources/sinks of Berry curvature except the gap-closing points (punctured-Chern invariant $(0, 0)$). For Eq. 3, they are at high-symmetry points $((0, \pi), (\pi, 0), (\pi, \pi))$ in Fig 2(d); also $(0, 0)$ in other cases) *away* from the gap-closing points (green dots). The punctured-Chern invariant captures them systematically akin to the Chern invariant for gapped bands. Thus, similar to quantized anomalous Hall transport [9], punctured-Chern gapless topology can drive *non-quantized* anomalous transport (c.f. Eqns. 3,4 of Ref. 50) constituting a physical effect of fragile topological bands [51].

Going now towards $3d$, we constructively arrive at a $\mathbb{Z} \times \mathbb{Z}$ classification for $3d$ triple-point nodes (Fig. 3). The three bands involved in the Nexus point must have (some multiple of) half-integer punctured-Chern numbers in the presence of linear band-crossings [52]. The sum of the

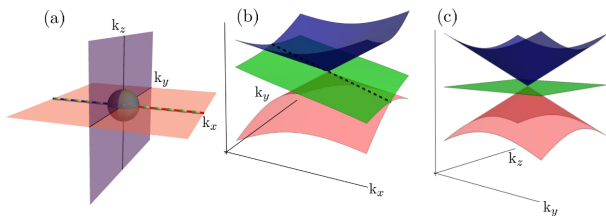


FIG. 3. a $3d$ Nexus triple-point with two doubly-degenerate nodal-lines emanating from the triple-point. Any surface (e.g. the shown sphere) surrounding the triple-point gets punctured by the nodal lines. (b) shows a chosen $2d$ projection containing the nodal-lines (light red plane in (a)). Other projections without the nodal-lines (e.g., purple plane in (a)) look like (c). A three-fold degenerate point that lacks the Nexus structure of (b) in any projection is an example of a “spin-1” chiral fermion.

punctured-Chern numbers over the three bands must be an integer, and zero if filling the three bands yield the trivial case, which is a natural expectation in many cases [53]. This implies there are only two independent half-integers. As half-integers map to \mathbb{Z} , therefore the classification of triple-points is $\mathbb{Z} \times \mathbb{Z}$ and computable via the punctured-Chern invariant. This invariant is appropriate for a specific choice of internal symmetries. Either time reversal or particle-hole may be present, but not both together. More generally, we restrict ourselves to the case when *all* the internal symmetries map (the vicinity of) the Nexus point to a different Nexus point, implying that there is *at least one distinct partner* of the Nexus triple-point. A rationale for this restriction will be given after discussing the main results. This distinct symmetry-related partner existence (DSPE) condition then excludes a Nexus point at the Γ point, but does not restrict to only a single pair of Nexus points.

The above $\mathbb{Z} \times \mathbb{Z}$ classification result can be derived using abstract algebra, which is conceptually independent of the existence of a constructive invariant. The general idea is to use exact sequences to calculate the homotopy groups of the mappings [54, 55] that are relevant to the Nexus (single-particle) band topology. A more familiar (many-body) example would be the classes of mappings relevant for a filled subset of gapped bands mapped onto a general sphere in the sought-after dimension [5, 56]. Its group structure is achieved by analyzing the constraints on it due to elements on either side of the corresponding long exact sequence [55]. The “periodic table” classification of topological insulators was similarly achieved using long exact sequences (e.g., Hopf fibration [56, 57]). A single-particle example would be a set of non-degenerate single-particle bands, say three bands, whose manifold structure would be described by the flag manifold $\text{Fl}_3 \simeq \text{U}(3)/\text{U}(1)^3$. For such a manifold, we can conclude $\pi_2(\text{Fl}_3) = \mathbb{Z} \times \mathbb{Z}$ using the corresponding long-exact sequence by exploiting its fibration structure as briefly described in Ref. 58.

Here, we have additional structure on the single-particle Nexus bands due to the emanating nodal-lines. The presence of gapless points on the manifold induces the antipodal boundary condition described previously which does not yield a simple fibration structure. This prevents directly writing down a long-exact sequence. To handle this, we treat the classification problem using homotopy pullback [59], and thereby construct a fibration on the space of mappings from the vicinity of the triple-point to the band manifold and use its long exact sequence [55, 60, 61] to unravel the classification. This leads to the $\mathbb{Z} \times \mathbb{Z}$ homotopy group for the band manifolds surrounding the Nexus triple-point (for details [58]).

Next, we discuss a model realization of the above ideas. To obtain a model consistent with DSPE, we take a $2d$ model of spinless electrons with three bands and time-reversal symmetry that has the Nexus structure with fine-tuned parameters [62, 63], and build up into $3d$. To stabilize the triple-point, we consider a crystalline system with C_{3v} ditrigonal pyramidal symmetry and a sublattice anti-symmetry Π . We note that the Type-B class of Table I in Ref. [30], especially those based on trigonal space groups (156-161), can provide promising candidates if the Fermi energy lies near the triple-points. We further assume that chiral symmetry is broken (following DSPE), and also broken reflection symmetry, but the product $\Pi\sigma_v$ is unbroken. Thus, the (anti-)symmetries act on the momenta as follows,

$$O_{C_3} = \begin{pmatrix} \cos \frac{2\pi}{3} & -\sin \frac{2\pi}{3} & 0 \\ \sin \frac{2\pi}{3} & \cos \frac{2\pi}{3} & 0 \\ 0 & 0 & 1 \end{pmatrix}, \quad O_{\Pi\sigma_v} = \begin{pmatrix} -1 & 0 & 0 \\ 0 & 1 & 0 \\ 0 & 0 & 1 \end{pmatrix}, \quad (4)$$

such that $gH(\mathbf{k})g^{-1} = H(O_g\mathbf{k})$, with g and O_g being representations of the symmetry transformation in the Hilbert space and the momentum space respectively. The following are their actions on the Hilbert space,

$$C_3 = \begin{pmatrix} e^{\frac{2\pi i}{3}} & 0 & 0 \\ 0 & e^{-\frac{2\pi i}{3}} & 0 \\ 0 & 0 & 1 \end{pmatrix}, \quad \Pi\sigma_v = \begin{pmatrix} 0 & 1 & 0 \\ 1 & 0 & 0 \\ 0 & 0 & 1 \end{pmatrix}. \quad (5)$$

For a generic point \mathbf{k}_o on the three-fold rotational (C_3) symmetry axis (chosen along the z -direction ($\mathbf{k}_o = k_z \hat{z}$)), the most generic Hamiltonian can be linearized in its vicinity ($\mathbf{p} \equiv \mathbf{k} - \mathbf{k}_o$):

$$H(\mathbf{p}) = \begin{pmatrix} \alpha p_z - \epsilon & \beta(p_x + ip_y) & \zeta(p_x - ip_y) \\ \beta(p_x - ip_y) & \epsilon - \alpha p_z & \zeta(p_x + ip_y) \\ \zeta^*(p_x + ip_y) & \zeta^*(p_x - ip_y) & 0 \end{pmatrix}. \quad (6)$$

Here, α , β , and ϵ are real parameters, and ζ is a complex parameter dependent on \mathbf{k}_o , i.e. $\alpha \equiv \alpha(\mathbf{k}_o)$, $\beta \equiv \beta(\mathbf{k}_o)$, $\zeta \equiv \zeta(\mathbf{k}_o)$ and $\epsilon \equiv \epsilon(\mathbf{k}_o)$. In the presence of a constant electric field parallel to the C_3 -axis given by the vector potential, $\mathbf{A}(t) = Et \hat{z}$, we get the following time-

Parameters	Range	puncture-Chern number
β, ζ	$ \beta < \zeta $	$(-2, 0, 2)$
	$ \beta = \zeta $	$(-1/2, 0, 1/2)$
	$ \beta > \zeta $	$(1, 0, -1)$

TABLE I. The Chern numbers for the three bands in three different parameter regimes for the Hamiltonian of Eq. 7 when the ϵ gets canceled. For $|\beta| = |\zeta|$ with a Nexus triple-point, we get a half-integer punctured-Chern set defined on the punctured manifold.

dependent Hamiltonian after minimal substitution,

$$H(\mathbf{p}, t) = \begin{pmatrix} \alpha p_z + \alpha e E t - \epsilon & \beta(p_x + i p_y) & \zeta(p_x - i p_y) \\ \beta(p_x - i p_y) & \epsilon - \alpha p_z - \alpha e E t & \zeta(p_x + i p_y) \\ \zeta^*(p_x + i p_y) & \zeta^*(p_x - i p_y) & 0 \end{pmatrix}. \quad (7)$$

Assuming a small field, we apply the adiabatic approximation, such that at time $t = \frac{\epsilon(\mathbf{k}_0)}{\alpha e E}$, the corresponding point \mathbf{k}_0 would become an isolated three-fold degenerate point (as in Fig. 3(c)). Since this is true for any point on the C_3 -axis, some point \mathbf{k}_0^* may generically also have the property that $|\beta| = |\zeta|$. Thus at t^* corresponding to \mathbf{k}_0^* , a triple-point is obtained at \mathbf{k}_0^* with three emanating *linear* nodal-lines. It is thus characterized by a half-integer punctured-Chern invariant as summarized in Table I.

Alternately, since the eigenvalues of rotation symmetry representations are complex (Eq. 5 involving C_3), this implies that the wavefunctions transform as (orbital) angular momentum $L = 1$ (also reflected in the diagonal entries of Eq. 6). We may thus apply a constant magnetic field B along the C_3 -axis, which will Zeeman couple as $B_z L_z$. If this term were to dominate over minimal coupling terms, then the Hamiltonian becomes essentially as in Eq. 7 with $\alpha e E t \rightarrow \mu_0 B$. Thus, we will again get triple-points with half-integer punctured-Chern numbers when $B = \epsilon(\mathbf{k}_0^*)/\mu_0$ (Table I). One can understand the half-integer nature of the punctured-Chern set as a topological transition [64, 65] between two three-fold chiral fermion phases with integer Chern numbers that are an odd integer apart [66]. We can finally write a tight-binding model based on the above with the following replacements

$$(p_x + i p_y) \rightarrow \sum_{\ell} e^{\frac{2\pi i \ell}{3}} \sin(\mathbf{a}_1 \cdot O_{C_3}^{-\ell} \mathbf{k}) \quad (8a)$$

$$\epsilon \rightarrow \eta \sum_{\ell} \cos(\mathbf{a}_1 \cdot O_{C_3}^{-\ell} \mathbf{k}) \quad (8b)$$

involving C_3 , and $\alpha p_z \rightarrow \epsilon(k_z)$, $\beta \rightarrow \beta(k_z)$, $\zeta \rightarrow \zeta(k_z)$. Here $\ell \in \{1, 2, 3\}$, \mathbf{a}_1 is the primitive lattice vector in the x -direction, η is a real parameter, $\epsilon(k_z)$ is a real function of k_z , and $\beta(k_z)$ and $\zeta(k_z)$ are respectively real and complex functions of k_z whose absolute values can intersect at some generic momentum (see Ref. 58 for the explicit formula).

The $\mathbb{Z} \times \mathbb{Z}$ topological invariant delineated in this paper

can be applied to non-electronic Nexus points in optical [65, 67] or phononic [68] band-structures. We note here that in other electronic Nexus triple-point models [30, 34], there are quadratic (instead of linear) band-touchings. For a quadratic band-touching, the antipodal condition gets lifted which leads back to a flag manifold of dimension 3. With DSPE, the classification will thus be $\pi_2(\mathbb{F}_3)$ which is again $\mathbb{Z} \times \mathbb{Z}$ given by integer Chern sets. For Ref. 34 and the type-A class of Ref. 30, there is a symmetry (time reversal times c -axis reflection) which does not satisfy DSPE. The Berry connection will thus get further “constrained” in the vicinity of Nexus point. This makes the punctured-Chern invariant inapplicable for these cases [69]. It is known that such DSPE-violating symmetries affect the classification [16] and thereby the topological invariants.

We conclude by discussing the relationship between the punctured-Chern invariant for Nexus band topology and physical quantities. Because of DSPE, we expect at least another “partner” Nexus point in the \mathcal{BZ} . Thus we expect that there will be Fermi arcs on the surface [70], details depend on their punctured-Chern numbers. Due to the half-integral nature from an odd number of nodal-lines, appropriate surface cuts will show “half-integral conductance” per cut (in units of e^2/h). An equivalent effect is a half-integral anomalous Hall contribution when the chemical potential is nearby a Nexus point [50]. When it is slightly below (above) the Nexus point, the Fermi surface consists of two hole (electron) Fermi pockets that linearly touch each other on the nodal-lines. This gives a Hall conductance that depends on the curvature integral over the two pockets and the connection integral to their boundaries (the infinitesimal loop at the puncture as in Fig. 1) [71]. The boundary terms cancel out, while the total curvature integral will equal that of the bottom (top) sphere, which is a half-integer [72].

The gapless methods involving punctured manifolds provide a new perspective and calculational tools for topological semi-metals. In the context of $3d$ Nexus triple-points, our methods go through in presence of certain symmetries as described before. This opens up questions regarding topological invariants to characterize Nexus points beyond the DSPE condition. This will indeed be necessary for several existing triple-point semi-metal candidates [73] including the type-A class in Table I of Ref. [30]. More generally, the utility of the punctured-Chern invariant lies in the fact that it can naturally capture semi-metallic band topology as seen for the $2d$ fragile topological model of Eq. 3. Another potential application could be to nodal-line semi-metals, where the punctured-Chern invariant can capture either fragile or stable topology in the background of the nodal lines in a $3d$ \mathcal{BZ} similar in spirit to Wilson loop eigenvalue characterization of topological insulators [74].

The authors acknowledge fruitful discussions with S. Carmeli, T. Holder, E. Berg, A. Stern, J. S. Hofmann.

AD was supported by the German-Israeli Foundation Grant No. I-1505-303.10/2019, and CRC 183 (project C01). A.D. also thanks the Israel planning and budgeting committee (PBC) and the Weizmann Institute of Science, the Dean of Faculty fellowship, and the Koshland Foundation for financial support. E.C. was supported by the Deutsche Forschungsgemeinschaft (DFG, German Research Foundation) project grant 277101999 within the CRC network TRR 183. S.P. acknowledges financial support from SERB-DST, India via grant no. SRG/2019/001419, and in the final stages of writing by grant no. CRG/2021/003024.

* ankur.das@weizmann.ac.il

† sumiran@phy.iitb.ac.in

- [1] M. Z. Hasan and C. L. Kane, *Rev. Mod. Phys.* **82**, 3045 (2010), URL <https://link.aps.org/doi/10.1103/RevModPhys.82.3045>.
- [2] M. Z. Hasan and J. E. Moore, *Annual Review of Condensed Matter Physics* **2**, 55 (2011), URL <https://doi.org/10.1146/annurev-conmatphys-062910-140432>.
- [3] X.-L. Qi and S.-C. Zhang, *Rev. Mod. Phys.* **83**, 1057 (2011), URL <https://link.aps.org/doi/10.1103/RevModPhys.83.1057>.
- [4] Y. Ando, *Journal of the Physical Society of Japan* **82**, 102001 (2013), URL <https://doi.org/10.7566/JFJPSJ.82.102001>.
- [5] B. A. Bernevig, *Topological insulators and topological superconductors* (Princeton university press, 2013).
- [6] A. W. W. Ludwig, *Physica Scripta* **T168**, 014001 (2015), URL <https://doi.org/10.1088/2F0031-8949/2F2015/2Ft168/2F014001>.
- [7] A. Stern, *Annual Review of Condensed Matter Physics* **7**, 349 (2016), URL <https://doi.org/10.1146/annurev-conmatphys-031115-011559>.
- [8] Y. Tokura, K. Yasuda, and A. Tsukazaki, *Nature Reviews Physics* **1**, 126 (2019), ISSN 2522-5820, URL <https://doi.org/10.1038/s42254-018-0011-5>.
- [9] D. J. Thouless, M. Kohmoto, M. P. Nightingale, and M. den Nijs, *Phys. Rev. Lett.* **49**, 405 (1982), URL <https://link.aps.org/doi/10.1103/PhysRevLett.49.405>.
- [10] A. Altland and M. R. Zirnbauer, *Phys. Rev. B* **55**, 1142 (1997), URL <https://link.aps.org/doi/10.1103/PhysRevB.55.1142>.
- [11] A. P. Schnyder, S. Ryu, A. Furusaki, and A. W. W. Ludwig, *Phys. Rev. B* **78**, 195125 (2008), URL <https://link.aps.org/doi/10.1103/PhysRevB.78.195125>.
- [12] S. Ryu, A. P. Schnyder, A. Furusaki, and A. W. W. Ludwig, *New Journal of Physics* **12**, 065010 (2010), URL <https://doi.org/10.1088/2F1367-2630/2F12/2F6/2F065010>.
- [13] A. Kitaev, V. Lebedev, and M. Feigel'man, in *AIP Conference Proceedings* (AIP, 2009), URL <https://doi.org/10.1063/2F1.3149495>.
- [14] L. Lu, J. D. Joannopoulos, and M. Soljačić, *Nature Photonics* **8**, 821 (2014), URL <https://doi.org/10.1038/2Fnpht.2014.248>.
- [15] E. Cornfeld and A. Chapman, *Phys. Rev. B* **99**, 075105 (2019), URL <https://link.aps.org/doi/10.1103/PhysRevB.99.075105>.
- [16] E. Cornfeld and S. Carmeli, *Phys. Rev. Research* **3**, 013052 (2021), URL <https://link.aps.org/doi/10.1103/PhysRevResearch.3.013052>.
- [17] C. L. Kane and E. J. Mele, *Phys. Rev. Lett.* **95**, 146802 (2005), URL <https://link.aps.org/doi/10.1103/PhysRevLett.95.146802>.
- [18] C. L. Kane and E. J. Mele, *Phys. Rev. Lett.* **95**, 226801 (2005), URL <https://link.aps.org/doi/10.1103/PhysRevLett.95.226801>.
- [19] O. Vafek and A. Vishwanath, *Annual Review of Condensed Matter Physics* **5**, 83 (2014), <https://doi.org/10.1146/annurev-conmatphys-031113-133841>, URL <https://doi.org/10.1146/annurev-conmatphys-031113-133841>.
- [20] H. C. Po, L. Zou, A. Vishwanath, and T. Senthil, *Phys. Rev. X* **8**, 031089 (2018), URL <https://link.aps.org/doi/10.1103/PhysRevX.8.031089>.
- [21] L. Zou, H. C. Po, A. Vishwanath, and T. Senthil, *Phys. Rev. B* **98**, 085435 (2018), URL <https://link.aps.org/doi/10.1103/PhysRevB.98.085435>.
- [22] Z. Song, Z. Wang, W. Shi, G. Li, C. Fang, and B. A. Bernevig, *Phys. Rev. Lett.* **123**, 036401 (2019), URL <https://link.aps.org/doi/10.1103/PhysRevLett.123.036401>.
- [23] H. C. Po, L. Zou, T. Senthil, and A. Vishwanath, *Phys. Rev. B* **99**, 195455 (2019), URL <https://link.aps.org/doi/10.1103/PhysRevB.99.195455>.
- [24] H. C. Po, H. Watanabe, and A. Vishwanath, *Phys. Rev. Lett.* **121**, 126402 (2018), URL <https://link.aps.org/doi/10.1103/PhysRevLett.121.126402>.
- [25] J. Ahn, S. Park, and B.-J. Yang, *Phys. Rev. X* **9**, 021013 (2019), URL <https://link.aps.org/doi/10.1103/PhysRevX.9.021013>.
- [26] A. Bouhon, A. M. Black-Schaffer, and R.-J. Slager, *Phys. Rev. B* **100**, 195135 (2019), URL <https://link.aps.org/doi/10.1103/PhysRevB.100.195135>.
- [27] B. Bradlyn, Z. Wang, J. Cano, and B. A. Bernevig, *Phys. Rev. B* **99**, 045140 (2019), URL <https://link.aps.org/doi/10.1103/PhysRevB.99.045140>.
- [28] A. M. Turner, E. Berg, and A. Stern, *Phys. Rev. Lett.* **128**, 056801 (2022), URL <https://link.aps.org/doi/10.1103/PhysRevLett.128.056801>.
- [29] T. T. Heikkilä and G. E. Volovik, *New Journal of Physics* **17**, 093019 (2015), ISSN 1367-2630, URL <http://dx.doi.org/10.1088/1367-2630/17/9/093019>.
- [30] Z. Zhu, G. W. Winkler, Q. Wu, J. Li, and A. A. Soluyanov, *Phys. Rev. X* **6**, 031003 (2016), URL <https://link.aps.org/doi/10.1103/PhysRevX.6.031003>.
- [31] H. Weng, C. Fang, Z. Fang, and X. Dai, *Phys. Rev. B* **93**, 241202 (2016), URL <https://link.aps.org/doi/10.1103/PhysRevB.93.241202>.
- [32] H. Weng, C. Fang, Z. Fang, and X. Dai, *Phys. Rev. B* **94**, 165201 (2016), URL <https://link.aps.org/doi/10.1103/PhysRevB.94.165201>.
- [33] T. Hyart and T. T. Heikkilä, *Phys. Rev. B* **93**, 235147 (2016), URL <https://link.aps.org/doi/10.1103/PhysRevB.93.235147>.
- [34] G. Chang, S.-Y. Xu, S.-M. Huang, D. S. Sanchez, C.-H. Hsu, G. Bian, Z.-M. Yu, I. Belopolski, N. Alidoust, H. Zheng, et al., *Scientific Reports* **7**, 1688 (2017), ISSN 2045-2322, URL <https://doi.org/10.1038/s41598-017-01523-8>.

- [35] X. Zhang, Z.-M. Yu, X.-L. Sheng, H. Y. Yang, and S. A. Yang, Phys. Rev. B **95**, 235116 (2017), URL <https://link.aps.org/doi/10.1103/PhysRevB.95.235116>.
- [36] X. Feng, C. Yue, Z. Song, Q. Wu, and B. Wen, Phys. Rev. Materials **2**, 014202 (2018), URL <https://link.aps.org/doi/10.1103/PhysRevMaterials.2.014202>.
- [37] C. K. Barman, C. Mondal, B. Pathak, and A. Alam, Phys. Rev. B **99**, 045144 (2019), URL <https://link.aps.org/doi/10.1103/PhysRevB.99.045144>.
- [38] P. M. Lenggenhager, X. Liu, S. S. Tsirkin, T. Neupert, and T. Bzdušek, Phys. Rev. B **103**, L121101 (2021), URL <https://link.aps.org/doi/10.1103/PhysRevB.103.L121101>.
- [39] B. Q. Lv, Z.-L. Feng, Q.-N. Xu, X. Gao, J.-Z. Ma, L.-Y. Kong, P. Richard, Y.-B. Huang, V. N. Strocov, C. Fang, et al., Nature **546**, 627 (2017), ISSN 1476-4687, URL <https://doi.org/10.1038/nature22390>.
- [40] J.-Z. Ma, J.-B. He, Y.-F. Xu, B. Q. Lv, D. Chen, W.-L. Zhu, S. Zhang, L.-Y. Kong, X. Gao, L.-Y. Rong, et al., Nature Physics **14**, 349 (2018), ISSN 1745-2481, URL <https://doi.org/10.1038/s41567-017-0021-8>.
- [41] J. Krempaský, L. Nicolaï, M. Gmitra, H. Chen, M. Fanciulli, E. B. Guedes, M. Caputo, M. Radović, V. V. Volobuev, O. c. v. Caha, et al., Phys. Rev. Lett. **126**, 206403 (2021), URL <https://link.aps.org/doi/10.1103/PhysRevLett.126.206403>.
- [42] J. Ahn, D. Kim, Y. Kim, and B.-J. Yang, Phys. Rev. Lett. **121**, 106403 (2018), URL <https://link.aps.org/doi/10.1103/PhysRevLett.121.106403>.
- [43] Q. Wu, A. A. Soluyanov, and T. Bzdušek, Science **365**, 1273–1277 (2019), ISSN 1095-9203, URL <http://dx.doi.org/10.1126/science.aau8740>.
- [44] A. Bouhon, Q. Wu, R.-J. Slager, H. Weng, O. V. Yazyev, and T. Bzdušek, Nature Physics **16**, 1137 (2020), ISSN 1745-2481, URL <https://doi.org/10.1038/s41567-020-0967-9>.
- [45] P. M. Lenggenhager, X. Liu, T. Neupert, and T. Bzdušek, Phys. Rev. B **106**, 085129 (2022), URL <https://link.aps.org/doi/10.1103/PhysRevB.106.085129>.
- [46] P. M. Lenggenhager, X. Liu, T. Neupert, and T. Bzdušek, Phys. Rev. B **106**, 085128 (2022), URL <https://link.aps.org/doi/10.1103/PhysRevB.106.085128>.
- [47] A. Das and S. Pujari, Phys. Rev. B **102**, 235148 (2020), URL <https://link.aps.org/doi/10.1103/PhysRevB.102.235148>.
- [48] R. Buzano and H. T. Nguyen, The Journal of Geometric Analysis **29**, 1043–1074 (2018), ISSN 1559-002X, URL <http://dx.doi.org/10.1007/s12220-018-0029-z>.
- [49] It is also known as the Riemann sphere, or the complex projective line $\mathbb{C}P^1$ in some contexts.
- [50] F. D. M. Haldane, Phys. Rev. Lett. **93**, 206602 (2004), URL <https://link.aps.org/doi/10.1103/PhysRevLett.93.206602>.
- [51] A more speculative question is if there can exist $2d$ models that have stable as opposed to fragile topology in presence of gap-closing.
- [52] In presence of quadratic band-touchings, the bands will have integer Chern numbers. One way to think of a quadratic band-touching is as two linear band-crossings of the same chirality or winding on top of each other.
- [53] Note the emanating nodal lines involve the top/middle band pair and middle/bottom pair symmetrically on either side as in Fig. 3.
- [54] J. R. Munkres, *Topology: a first course* (Prentice-Hall, 1974).
- [55] M. Artin, *Algebra* (Pearson Education, Boston, MA, 2011), ISBN 978-0132413770.
- [56] M. Stone and P. Goldbart, *Mathematics for physics* (Cambridge University Press, Cambridge, England, 2009).
- [57] H. Hopf, Mathematische Annalen **95**, 313 (1926), URL <https://doi.org/10.1007/bf01206614>.
- [58] For further details, see Supplementary materials.
- [59] M. P. Carmo, *Differential geometry of curves and surfaces* (Dover Publications, Mineola, NY, 2016), 2nd ed.
- [60] M. Frankland (2013), URL https://www.home.uni-osnabrueck.de/mfrankland/Math527/Math527_0308.pdf.
- [61] A. Hatcher, C. U. Press, and C. U. D. of Mathematics, *Algebraic Topology*, Algebraic Topology (Cambridge University Press, 2002), ISBN 9780521795401, URL <https://books.google.co.il/books?id=BjKs86kosqgC>.
- [62] A. Das and S. Pujari, Phys. Rev. B **100**, 125152 (2019), URL <https://link.aps.org/doi/10.1103/PhysRevB.100.125152>.
- [63] A $2d$ aside: for the $2d$ Nexus triple-point in Ref. [62] that requires fine-tuning, a generalized winding number invariant was constructed to capture the $2d$ Nexus topology. See Sec. II and Table I of Ref. [62]. A non-Abelian Berry characterization can also be done for this $2d$ situation (see this link). These invariants do not lift naturally to $3d$ where triple-points can be stabilized via symmetry protection, which gives a counter-perspective on the punctured-Chern invariant constructed before.
- [64] A. Bouhon and R.-J. Slager, *Multi-gap topological conversion of euler class via band-node braiding: minimal models, pt-linked nodal rings, and chiral heirs* (2022), URL <https://arxiv.org/abs/2203.16741>.
- [65] F. N. Ünal, A. Bouhon, and R.-J. Slager, Phys. Rev. Lett. **125**, 053601 (2020), URL <https://link.aps.org/doi/10.1103/PhysRevLett.125.053601>.
- [66] The $2d$ semi-metallic bandstructure surrounding a Nexus triple point is also an example of stable topology in presence of gap closing ensconced in a $3d$ BZ .
- [67] S. Park, Y. Hwang, H. C. Choi, and B.-J. Yang, Nature Communications **12**, 6781 (2021), ISSN 2041-1723, URL <https://doi.org/10.1038/s41467-021-27158-y>.
- [68] M. Li, J. Song, and Y. Jiang, Phys. Rev. B **105**, 085304 (2022), URL <https://link.aps.org/doi/10.1103/PhysRevB.105.085304>.
- [69] We note that the punctured-Chern numbers are all zeros for Ref. [34]. See supplementary of this paper.
- [70] We have verified this for example cases as shown in the supplementary [58]. See section VA of Ref. 47 for some further discussion.
- [71] See in particular Eqns. 4, 21, and the final summary paragraph of Ref. 50.
- [72] There will also similarly be an integral anomalous Hall conductance contribution for the other entries in Table I.
- [73] G. W. Winkler, S. Singh, and A. A. Soluyanov, Chinese Physics B **28**, 077303 (2019), URL <https://doi.org/10.1088%2F1674-1056%2F28%2F7%2F077303>.
- [74] A. Alexandradinata, X. Dai, and B. A. Bernevig, Phys. Rev. B **89**, 155114 (2014), URL <https://link.aps.org/doi/10.1103/PhysRevB.89.155114>.

Supplementary to A $\mathbb{Z} \times \mathbb{Z}$ topological invariant for triple-point Nexus fermions

Ankur Das,¹ Eyal Cornfeld,¹ and Sumiran Pujari²

¹*Department of Condensed Matter Physics, Weizmann Institute of Science, Rehovot 7610001, Israel*

²*Department of Physics, Indian Institute of Technology Bombay, Mumbai, MH 400076, India*

Some details connected to the main text are presented here. We discuss the homotopy groups of the different manifolds and specifically the case of the punctured-manifolds associated with the three connected surrounding surfaces for Nexus triple-points. We also present a lattice version of the continuum model with Nexus points discussed in the main text based on the trigonal system, and we show Fermi arcs for a simpler model based on the cubic system.

Below, we present the abstract algebraic proof that the classification of Nexus triple-points with linear band-crossings in presence of the DSPE condition (see main text) is given by $\mathbb{Z} \times \mathbb{Z}$. We start with the simpler case of flag manifolds in Sec. I before going to the case of punctured Nexus manifolds in Sec. II. In Sec. III, we describe a lattice realization of the continuum model with Nexus points discussed in the main text (Eq. 7 of the same). In Sec IV, we show the Fermi arc behavior of a simpler lattice model based on a previous work¹.

I. HOMOTOPIES OF FLAG MANIFOLDS

We start with the the complex complete flag manifold, denoted by

$$\text{Fl}_3 \stackrel{\text{def}}{=} \text{U}(3)/\text{U}(1)^3 \simeq \text{SU}(3)/\text{U}(1)^2. \quad (1)$$

A fibration, $F \rightarrow E \rightarrow B$, satisfies²

$$\cdots \rightarrow \pi_{n+1}(B) \rightarrow \pi_n(F) \rightarrow \pi_n(E) \rightarrow \pi_n(B) \rightarrow \pi_{n-1}(F) \rightarrow \cdots \quad (2)$$

By $\text{U}(1)^2 \rightarrow \text{SU}(3) \rightarrow \text{Fl}_3$ we have

$$\begin{array}{ccccccccc} \pi_2(\text{SU}(3)) & \longrightarrow & \pi_2(\text{Fl}_3) & \longrightarrow & \pi_1(\text{U}(1)^2) & \longrightarrow & \pi_1(\text{SU}(3)) & \longrightarrow & \pi_1(\text{Fl}_3) & \longrightarrow & \pi_0(\text{U}(1)^2) \\ \parallel & & \vdots & & \parallel & & \parallel & & \vdots & & \parallel \\ 0 & \cdots & \mathbb{Z}^2 & \cdots & \mathbb{Z}^2 & \longrightarrow & 0 & \cdots & 0 & \cdots & 0 \end{array} \quad (3)$$

Here, the dashed arrows are deduced by the structure of the long exact sequence. We conclude that $\pi_1(\text{Fl}_3) = 0$ and $\pi_2(\text{Fl}_3) = \mathbb{Z}^2$.

II. THE THREE CONNECTED SPHERES

If Z is a connected space then the homotopy pullback³,

$$\begin{array}{ccc} & P & \\ & \swarrow & \searrow \\ X & & Y \\ & \searrow & \swarrow \\ & Z & \end{array} \quad (4)$$

is a fibration, $\Omega Z \rightarrow P \rightarrow X \times Y$, and $P = X \times_Z Y = \{(x, \gamma(t), y) : \gamma(0) = z(x), \gamma(1) = z(y)\}$.

A. Warmup: two connected spheres

Notice that $\text{Fl}_2 \simeq \mathbb{C}\mathbb{P}^1 \simeq S^2$.

The two connected spheres can be viewed as a disk $\partial(D^2) = S^1$. There is a \mathbb{Z}_2 -action on the boundary sphere which takes each point to its antipodal point. Under this action, the two basis vectors in \mathbb{F}_2 change places which is the antipodal action on \mathbb{CP}^1 .

Therefore there is a homotopy pullback

$$\begin{array}{ccc}
 & \text{Map}^{\text{Conditions}}(D^2, \mathbb{CP}^1) & \\
 \swarrow & & \searrow \\
 \text{Map}(D^2, \mathbb{CP}^1)_{*=\text{hemisphere}} & & \text{Map}_{\mathbb{Z}_2}(S^1, \mathbb{CP}^1) \\
 \searrow & & \swarrow \\
 & \text{Map}(S^1, \mathbb{CP}^1)_{*=\text{equator}} &
 \end{array} \tag{5}$$

such that the number of topologically distinct maps from the disc to \mathbb{CP}^1 that obey the antipodality conditions on the boundary are given by $\pi_0(P)$ with $P = \text{Map}^{\text{Conditions}}(D^2, \mathbb{CP}^1)$. The homotopy pullback must be defined relative to a selection of basepoints. For the spaces of maps from the disc to \mathbb{CP}^1 we pick as a basepoint the hemisphere map which maps a disc to one of the hemispheres.

The exact sequence reads

$$\begin{array}{ccccccc}
 \pi_1(X) \times \pi_1(Y) & \longrightarrow & \pi_0(\Omega Z) & \longrightarrow & \pi_0(P) & \longrightarrow & \pi_0(X) \times \pi_0(Y) \\
 \parallel & & \parallel & & \vdots & & \parallel \\
 0 \times \mathbb{Z} & \xrightarrow{0} & \mathbb{Z} & \cdots \cdots \cdots & \{\mathbb{Z}\} & \cdots \cdots \cdots & 0 \times 0
 \end{array} \tag{6}$$

We thus conclude that $\pi_0(P) = \mathbb{Z}$.

Check: We know that $\pi_0(P) = \pi_0(\text{Map}^{\text{Conditions}}(D^2, \mathbb{CP}^1)) = \pi_0(\text{Map}_{\mathbb{Z}_2}^{\text{antipodal}}(S^2, \mathbb{CP}^1)) = \{\mathbb{Z}\} - \{2\mathbb{Z}\}$ as labeled by the pushforward $\pi_2(S^2) \rightarrow \pi_2(\mathbb{CP}^1)$.

B. Calculation

The three connected spheres can be viewed as a cylinder $\partial(S^1 \times I) = S_u^1 \cup S_d^1$. On each sphere, one of the vectors $v_1 \perp v_2 \perp v_3 \in \mathbb{F}_3$ is constant. These vectors are thus points in $\mathbb{CP}^2 \subset \mathbb{F}_3$ and they restrict the other pairs to lie in the orthogonal $\mathbb{F}_2 \simeq \mathbb{CP}^1 \simeq S^2$. There is a \mathbb{Z}_2 -action on the boundary spheres which takes each point to its antipodal point. Under this action, the two free basis vectors in \mathbb{F}_3 change places. That is, for $x_{u,d} \in S_{u,d}^1$ we have

$$x_u; (v_1, v_2, v_3) \mapsto -x_u; (v_2, v_1, v_3), \tag{7}$$

$$x_d; (v_1, v_2, v_3) \mapsto -x_d; (v_1, v_3, v_2). \tag{8}$$

Therefore there is a homotopy pullback

$$\begin{array}{ccc}
 & \text{Map}^{\text{Conditions}}(S^1 \times I, \mathbb{F}_3) & \\
 \swarrow & & \searrow \\
 \text{Map}(S^1 \times I, \mathbb{F}_3) & & (\mathbb{CP}_{v_3}^2 \times \text{Map}_{\mathbb{Z}_2}(S_u^1, \mathbb{CP}_{v_1, v_2}^1)) \times (\mathbb{CP}_{v_1}^2 \times \text{Map}_{\mathbb{Z}_2}(S_d^1, \mathbb{CP}_{v_2, v_3}^1)) \\
 \searrow & & \swarrow \\
 & \text{Map}(S_u^1, \mathbb{F}_3) \times \text{Map}(S_d^1, \mathbb{F}_3) &
 \end{array} \tag{9}$$

such that the number of topologically distinct maps from the cylinder to \mathbb{CP}^2 that obey the antipodality conditions on the boundary are given by $\pi_0(P)$ with $P = \text{Map}^{\text{Conditions}}(S^1 \times I, \mathbb{F}_3)$. Here basepoints are picked akin to the previous section.

The exact sequence reads

$$\begin{array}{ccccccc}
\pi_1(X) \times \pi_1(Y) & \longrightarrow & \pi_0(\Omega Z) & \longrightarrow & \pi_0(P) & \longrightarrow & \pi_0(X) \times \pi_0(Y) \\
\parallel & & \parallel & & \vdots & & \parallel \\
\mathbb{Z}^2 \times ((0 \times \mathbb{Z}) \times (0 \times \mathbb{Z})) & \xrightarrow{\begin{pmatrix} 1 & 0 & 0 & 0 \\ 0 & 1 & 0 & 0 \\ 1 & 0 & 0 & 0 \\ 0 & 1 & 0 & 0 \end{pmatrix}} & \mathbb{Z}^2 \times \mathbb{Z}^2 & \cdots \longrightarrow & \{\mathbb{Z}^2\} & \cdots \longrightarrow & 0 \times 0
\end{array} \tag{10}$$

Thus, we finally conclude that $\pi_0(P) = \mathbb{Z}^2$.

III. LATTICE DETAILS

Here we write down the explicit formula for the tight-binding Hamiltonian starting from the continuum model that was described in the main text. It is

$$H(\mathbf{k}) = \begin{pmatrix} \epsilon(k_z) - \eta \sum_{\ell} \cos(\mathbf{R}_1 \cdot O_{C_3}^{-\ell} \mathbf{k}) & \beta(k_z) \sum_{\ell} e^{\frac{2\pi i \ell}{3}} \sin(\mathbf{R}_1 \cdot O_{C_3}^{-\ell} \mathbf{k}) & \zeta(k_z) \sum_{\ell} e^{\frac{2\pi i \ell}{3}} \sin(\mathbf{R}_1 \cdot O_{C_3}^{\ell} \mathbf{k}) \\ \beta(k_z) \sum_{\ell} e^{\frac{2\pi i \ell}{3}} \sin(\mathbf{R}_1 \cdot O_{C_3}^{\ell} \mathbf{k}) & -\epsilon(k_z) + \eta \sum_{\ell} \cos(\mathbf{R}_1 \cdot O_{C_3}^{-\ell} \mathbf{k}) & \zeta(k_z) \sum_{\ell} e^{\frac{2\pi i \ell}{3}} \sin(\mathbf{R}_1 \cdot O_{C_3}^{-\ell} \mathbf{k}) \\ \zeta^*(k_z) \sum_{\ell} e^{\frac{2\pi i \ell}{3}} \sin(\mathbf{R}_1 \cdot O_{C_3}^{\ell} \mathbf{k}) & \zeta^*(k_z) \sum_{\ell} e^{\frac{2\pi i \ell}{3}} \sin(\mathbf{R}_1 \cdot O_{C_3}^{\ell} \mathbf{k}) & 0 \end{pmatrix}, \tag{11}$$

where $\ell \in \{1, 2, 3\}$, \mathbf{R}_1 is the primitive lattice vector in the r_1 direction, η is a real parameter, $\epsilon(k_z)$ is a real function of k_z , and $\beta(k_z)$ and $\zeta(k_z)$ are respectively real and complex functions of k_z whose absolute values intersect at some generic momentum (one may choose one but not both to be constant functions). If one denotes by k'_z the momentum which satisfies $|\beta(k'_z)| < |\zeta(k'_z)|$ the triple-point transition would occur at magnetic fields $B = [3\eta - \epsilon(k'_z)]/\mu$. This model is inspired by those in Ref. 1, specifically the Λ_3 modification in the k_z direction, however with the C_3 symmetry axis lying along k_z as well. In Fig. 1, we show the bulk bandstructure for this model with $|\beta| = |\zeta|$ along the high symmetry lines in the Brillouin zone. Note that 1) the triple point is on the Γ - A axis as expected as per the discussion in the main text, since it is also the C_3 -axis as well, and 2) the double degeneracy seen on the Γ - K axis is actually a consequence of one of the three C_3 -symmetry related nodal lines which emerge from the triple point intersecting with this axis.

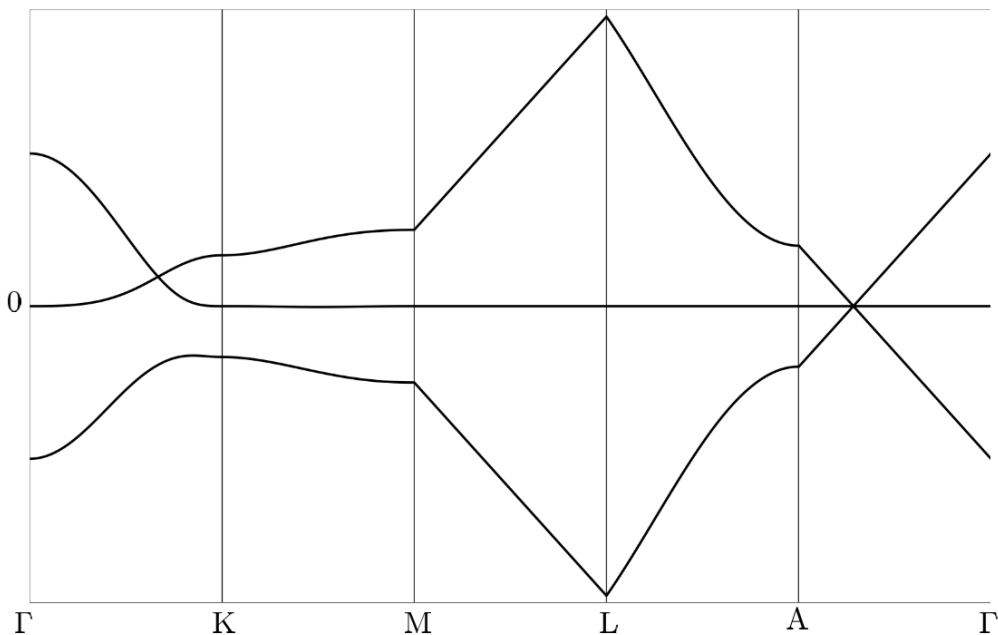


FIG. 1. Bulk energy spectrum for the lattice model in Eq. 11 along the high symmetry lines.

IV. FERMI ARCS

To illustrate the Fermi arcs due to the topological character of the triple points, we choose a simpler model based on our previous work (Ref. 1):

$$H(\mathbf{p}) = \begin{pmatrix} p_z & p_x - ip_y & p_x - ip_y \\ p_x + ip_y & -p_z & p_x + ip_y \\ p_x + ip_y & p_x - ip_y & 0 \end{pmatrix}. \quad (12)$$

and lift it to a cubic lattice system by the following replacements: $p_z \rightarrow \sin k_z$, $p_y \rightarrow \sin k_y$, and $p_x \rightarrow 2 - \cos k_x - \cos k_y - \cos k_z$. This leads to the Fermi arcs on $(0, 0, 1)$ plane as seen in Fig. 2.

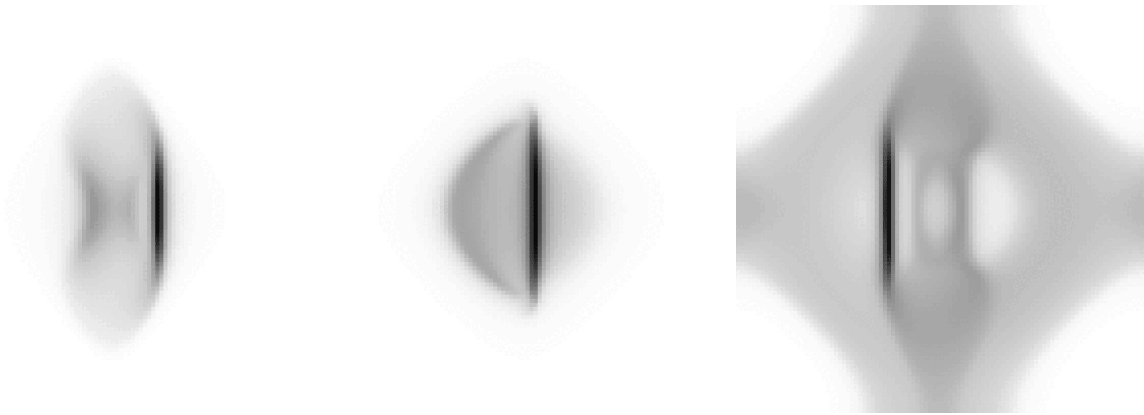


FIG. 2. From left to right, we present equal energy surface state density at three different increasing energies, which shows the Fermi arc structure connecting two pockets.

¹ A. Das and S. Pujari, Phys. Rev. B **102**, 235148 (2020), URL <https://link.aps.org/doi/10.1103/PhysRevB.102.235148>.

² A. Hatcher, C. U. Press, and C. U. D. of Mathematics, *Algebraic Topology*, Algebraic Topology (Cambridge University Press, 2002), ISBN 9780521795401, URL <https://books.google.co.il/books?id=BjKs86kosqG>.

³ M. Frankland (2013), URL https://www.home.uni-osnabrueck.de/mfrankland/Math527/Math527_0308.pdf.